

---

## Metal-halide lamps at microgravity, experiments and model

---

**Abstract.** The results from optical emission spectroscopy experiments of metal-halide lamps under the micro-gravity conditions on board the international space station are compared to the results of a numerical LTE model constructed with the platform Plasimo. At micro-gravity there is no convection which allows for easier modelling and for a separate study of the diffusion-induced radial segregation effect, undisturbed by convection. The plasma parameters that were experimentally determined and compared to the model were the Dy atom and ion density, the Hg ion density and the temperature.

The model and experiments applied to a reference lamp burning on a plasma mixture of DyI<sub>3</sub> and Hg were found to be in reasonable agreement with each other. The cross-section for electron-Hg collisions was studied, it was found that the Rockwood values give the correct results. Experimental results guided a sensitivity analysis of the model for the Langevin cross-sections. The ratio of the ion densities  $Hg^+/Dy^+$  was found to be extremely sensitive for the cross section of the elastic interaction  $\sigma(Hg, Dy^+)$  between the Dy ion and the Hg atom. The sensitivity analysis suggests that equating  $\sigma(Hg, Dy^+)$  to a value that is 10% higher than the Langevin cross-section is the best choice. We also found deviations from LTE in the outer regions of the plasma for relative radial positions of  $r/R > 50\%$ .

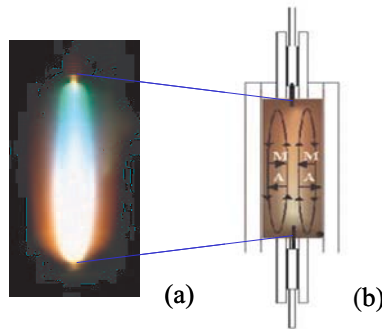


**Figure 5.1:** (a) Colour separation in a metal-halide lamp burner. (b) Schematic view of a metal-halide lamp; diffusion and convection of atoms (A) and molecules (M) are indicated by arrows. See figure 1.1 for full colour.

## 5.1 Introduction

The metal-halide lamp [1–3] combines the high luminous efficacy and good colour rendering of the fluorescent lamp with the compact and high-power characteristics of the high-pressure Hg lamps. The lamp contains a rare gas for starting and a Hg buffer gas plus a small amount of metal-halide additives such as  $\text{DyI}_3$ ,  $\text{TlI}$ , or  $\text{NaI}$ . Even though the additive density is much less than the mercury density, most light is emitted by the metals in the visible region, which results in a very high power efficiency (up to 40%). However, despite the clear advantages the growth of the metal-halide lamp has been hampered by a number of limitations. One of these is the segregation of colours [4] caused by the non-uniform distribution of the additives over the lamp due to the competition between diffusive and convective processes, see figure 5.1.

To be able to unravel the complex interaction between convection and diffusion, experiments under micro-gravity conditions have been performed at the international space station. In absence of gravity, convection is eliminated, so that the effect of diffusion can be studied exclusively and the problem is greatly simplified. The metal-halide lamp in micro-gravity is therefore easier to model. By comparing the model results to the experiments we can gain insight into the complex transport phenomena in the metal-halide lamp. The experiments verify the model results, whereas the model aids the interpretation of the experimental results. The experiments are part of a poly-diagnostic study [5–11] of the metal-halide lamp.

In this paper we present the comparison between the experiments performed on metal-halide lamps under micro-gravity conditions and a numerical model. The experiments were performed in the micro-gravity environment of the international space station (ISS). The lamp was investigated by means of optical emission spectroscopy, which yields line intensities of the species Hg, Dy and  $\text{Dy}^+$ . From the calibrated Hg line intensity measurements we constructed radial temperature profiles. By combining the temperature profile with the calibrated line intensities for Dy we obtained absolute radial density distributions of the

Dy and  $\text{Dy}^+$  systems. All measurements were done for different powers ranging from 70 to 150 W. The results were reported in [9].

Metal-halide lamps come in various shapes and sizes. In order to cross-compare results of the various experiments done on metal-halide lamps and to compare the results from models to the experiments a reference lamp has been defined within the framework of the European project COST-529 [12]. The lamp was filled with an Hg buffer gas and one salt, i.e.  $\text{DyI}_3$ . This lamp has a relatively simple salt system and therefore the results are easier to compare with the results of the numerical model. We base our models on this lamp geometry. The simulation platform used to construct this model is called Plasimo and is described in [13–16]. The model simulated the lamp operating with the following conditions, an electrode distance of 18 mm, a power of 130 W and a Hg pressure of 12 bar.

There are a number of input-parameters that are not well known, such as the vapour pressure of the metal-halide salt at the cold-spot position, the transition probabilities and the cross-sections for the elastic collisions between charged and neutral particles. The latter is found to be determinative for the segregation phenomenon. The sensitivity of the model results for the elastic collisional cross-section for the Dy ion and Hg atom were tested. Because the cross-sections for the elastic collisions between the Dy ion and the Hg atom are unknown, the Langevin cross-section [17] was used. The sensitivity of this approximation is investigated.

This chapter is organized as follows. Section 5.2 describes the segregation phenomenon. Section 5.3 gives an account of the experiment. Section 5.4 illustrates the model. Results from both experiment and model are presented and discussed in section 5.5. These results include the comparison between model and experiment of the radial profiles of the arc temperature and absolute atomic and ionic densities of Dy. Finally, section 5.6 offers conclusions and recommendations for future work.

## 5.2 De-mixing

When the metal-halide lamp is operated, the Hg is entirely vaporised forming the buffer-gas, whereas the few milligrams of  $\text{DyI}_3$  additive does not evaporate completely, leaving a liquid salt pool at the coldest spot at the burner wall. The additive molecules diffuse from the relatively cool wall ( $\sim 1200$  K) toward the hot region ( $\sim 6000$  K) of the arc where they dissociate. At the centre the atoms are ionised and excited. As Dy atoms diffuse back to the wall they encounter I atoms in the cooler gas near the walls and recombine back to molecules [1].

Three principal regions can therefore be identified within the radial density distribution of elemental Dy [10] (see Figure 5.2). These are 1) the region near the wall where  $\text{DyI}_3$  molecules are predominant, 2) the mantle region between the wall and the arc core where Dy atoms predominate, and 3) the core where the Dy is almost completely ionized in the form of  $\text{Dy}^+$ . The molecules  $\text{DyI}_2$  and  $\text{DyI}$  are relatively unstable and do not have a dominant presence in any region of the discharge.

When burned vertically, the discharge emits light that is non-uniform in colour along it's

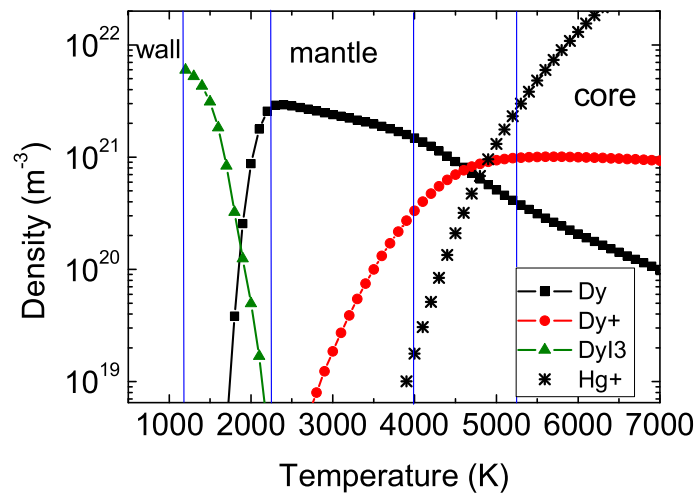


**Figure 5.2:** Theoretical density distribution of Dy atoms, ions and molecules, and Hg ions as a function of temperature at the midplane of a metal-halide lamp. For clarity, DyI<sub>2</sub> and DyI have been omitted.

axis. This colour segregation is caused by the interplay between convection and diffusion which ultimately determines the distribution of the plasma species. Let's first consider the radial distribution. The temperature profile, which is high in the centre and rapidly decreases towards the wall, leads to a hollow profile for the mass density distribution due to the ideal gas law. Another mechanism that influences the radial distribution of elemental Dy is diffusion. The atoms and molecules have different diffusion velocities. The smaller and lighter Dy atoms diffuse faster outward than the larger and heavier molecules (DyI, DyI<sub>2</sub>, DyI<sub>3</sub>) diffuse inward. This difference in diffusion velocity results, in steady-state, in an even more hollow profile of the elemental density of Dy; this effect is called radial segregation [4]. Ambipolar diffusion [19], in particular, causes the ions to diffuse out of the core faster than neutral atoms or molecules diffuse inwards.

The axial distribution of the species is dominated by convection, which causes the hot gas to move upwards in the hot centre of the arc and downwards along the cool wall of the lamp. This movement of the bulk gas drags the high concentration of elemental Dy near the wall downwards, whereas the lower concentration of Dy in the centre, caused by the radial segregation, is dragged upwards. As a consequence, a high density of elemental Dy accumulates at the bottom of the arc, a phenomenon which is known as axial segregation [4]. The combination of radial and axial segregation is shown in figure 5.1(b). The latter obviously only occurs in presence of convection. Since there is no convection under microgravity conditions axial segregation does not occur, but radial segregation does.

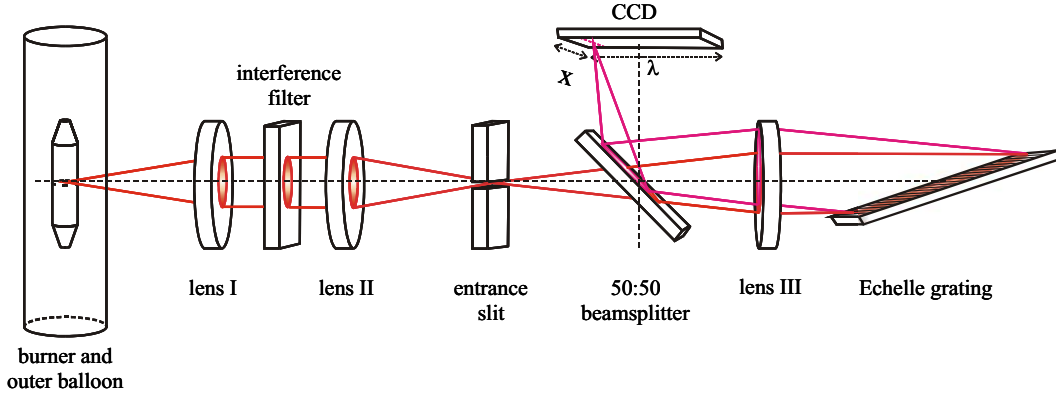


**Figure 5.3:** Setup used for the ISS measurements. It is an Echelle type spectrometer in Littrow configuration, the imaging lens (III) is used for the collimation of both the un-dispersed beam of light as well as the reflected dispersed beam of light.

### 5.3 The experiment

In the ISS experiment, emission spectroscopy was performed on a metal-halide lamp [12], which is, as mentioned above, a reference lamp. The lamp consists of a quartz burner of 20 mm in length and 8 mm in inner diameter and a transparent quartz vacuum outer bulb. The burner is made of quartz in order to make the arc optically accessible. The distance between the electrodes is approximately 18 mm. The lamp is driven by a 150 W Philips Dynavision DALI ballast with a 83 Hz square wave current profile, and operated at different input powers ranging from 70 to 150 W in steps of 20 W.

An Echelle-type spectrometer was used as there is need for a robust and compact setup with no moving parts for the experiments at micro-gravity. The downside is that only a few lines could be analysed. A schematic of the Echelle-type spectrometer is shown in figure 5.3 [9] [20]. Its main components are an Echelle grating with a high blaze angle ( $74^\circ$ ), an interference filter for the selection of the desired wavelength interval and a CCD camera for imaging. This spectrometer was used to measure the absolute intensity of three lines of three different systems. These are the 579.07 nm line of the atomic Hg system, the 642.19 nm and the 402.44 nm line of the atomic and ionic Dy system respectively; shortly denoted by the Dy and  $\text{Dy}^+$  system. The Hg line is used for the determination of the radial temperature distribution, and combined with the lines of Dy and  $\text{Dy}^+$  the densities of the Dy and  $\text{Dy}^+$  systems can be determined.

The procedure is as follows, first the transition-integrated intensity of the line emitting species is determined as a function of lateral position. After Abel inversion this gives the radiant power of the transition

$$U_{pq}(r) = n_p(r)A(p, q)h\nu_{pq} \quad (5.1)$$

from which,  $n_p(r)$ , the radial distribution of the radiating level can be determined since the transition probability  $A(p, q)$  and the photon energy  $h\nu_{pq}$  of the transition are known.

The density of the system to which radiating level belongs can now be determined using the Boltzmann relation [9] [18]

$$n_s(r) = \frac{U_{pq}(r)Q(T(r))}{g_p A(p, q) h\nu_{pq}} \exp\left(\frac{E_p}{kT(r)}\right), \quad (5.2)$$

where  $n_s$  is the system density of an emitting atom or ion,  $g_p$  the statistical weight of upper level  $p$ ,  $A(p, q)$  is the transition probability of the transition,  $h\nu_{pq}$  the energy of the emitted photon,  $E_p$  the excitation energy of the radiating level,  $k$  the Boltzmann constant and  $T$  is the temperature.  $Q(T)$  is the partition function of the considered atomic or ionic system.  $U_{pq}$  is the radiant power and determined experimentally, while  $Q(T)$ ,  $g_p$ ,  $A$  can be found in literature [23–25].

In case of the 579 nm transition of Hg this expression can be used to find the radial distribution of the temperature  $T(r)$ . This is done by replacing the left-hand-side of equation 5.2 by  $p/kT(r)$  which is justified since the atomic Hg system delivers the majority of particles in the lamp so that Daltons law,  $p = \sum nkT$ , reduces to  $p = n_{Hg(r)}kT(r)$ . This bulk pressure can be assumed to be constant over the lamp. Since  $U_{pq}(r)$  is known as a function of radial position we can use equation 5.2 to determine the temperature as a function of radial position provided the pressure is known. Since this is not the case we follow an iterative procedure. First a guessed value of  $p$  is inserted which gives, using the measured  $U_{pq}(r)$ , a radial  $T(r)$  distribution. In the second step we determine  $n_{Hg}(r) = p/kT(r)$  which, integrated over the whole volume, gives the total number of mercury atoms  $N_{Hg}$  in the discharge. In the last step this number, multiplied with the mass of a Hg atom, thus  $N_{Hg}m_{Hg}$ , is compared to the filling mass  $M_{Hg}$ . The mismatch  $M_{Hg}/N_{Hg}m_{Hg}$  is used to correct the pressure. With this new pressure-value we can repeat steps 1 till 3 again. This is done until convergence is reached.

Calculation of the radial density profiles is as follows. First the emission of the line of interest is measured as a function of lateral position. This profile is then Abel inverted into a radial intensity profile. The next step depends on the species of which the emission line is measured.

In case of the 579 nm line of Hg, the intensity is calibrated and then the absolute radial intensity profile is used to numerically determine the temperature profile. In case the atomic or ionic lines of Dy are measured, the temperature profile is combined with the calibrated radial intensity profile of the additive into an absolute radial system density profile using equation 5.2

## 5.4 The model

A description of the model has been published in [15] and [16] where it has been applied to a metal-halide lamp based on a mixture of Hg and NaI. In the following a brief summary is given in order to give an outline of the basic equations and to highlight changes made to the model since these publications. The most significant change is the substitution of NaI by DyI<sub>3</sub>.

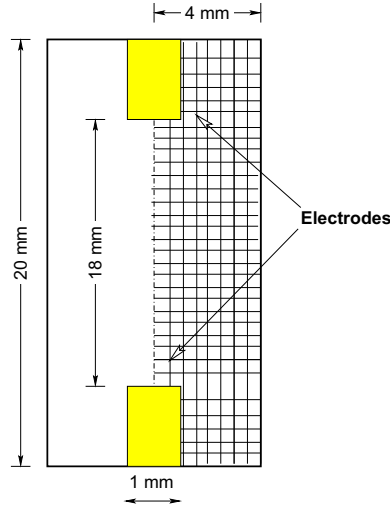


**Figure 5.4:** Schematic picture (not to scale) of the grid with respect to the inner burner.

### 5.4.1 Geometry of the problem

The model lamp has a distance between the electrodes of 18 mm, the length of the inner burner is 20 mm, and the diameter is 8 mm. We assume that the discharge is axially symmetric. The models thus use a two-dimensional rotationally symmetric grid. Figure 5.4 gives a schematic view of the geometry of the grid and the discharge. All equations are discretized on a structured finite volume mesh.

### 5.4.2 Basic equations

We will give a short overview of the basic equations solved in the model. More details are presented in [15] and [16]. The model assumes Local Thermal Equilibrium (LTE) [18]. The lamp is operated at a constant power of 130 W using a mixture of Hg and DyI<sub>3</sub>.

#### Energy balance

All modules come together in the energy balance to calculate the plasma temperature. The temperature, in turn, strongly influences the transport coefficients, composition, flow and radiation. The temperature is given by

$$\nabla \cdot (C_p \mathbf{v} \nabla T) - \nabla \cdot (\lambda_c \nabla T) = P + Q_{rad}, \quad (5.3)$$

where  $C_p$  is the heat capacity at constant pressure,  $\mathbf{v}$  the bulk velocity,  $\lambda_c$  the thermal conductivity,  $P = \sigma_{el} E^2$  the Ohmic dissipation, and  $Q_{rad}$  the energy source term due to radiation transport. Viscous energy source terms are neglected. The electrodes are assumed to have a surface temperature of 2900 K and the rest of the wall a temperature

of 1200 K. The term  $Q_{rad}$  is the result of 2D ray-tracing. We solve the equation for the radiation intensity  $I_\nu$  [26]

$$\frac{dI_\nu}{ds} = j_\nu - \kappa I_\nu, \quad (5.4)$$

with  $j_\nu$  the local emission coefficient and  $\kappa$  the local coefficient for absorption along rays passing through the discharge [16]. The radiation loss term is given by [26]:

$$Q_{rad} = \int_\nu \left( -4\pi j_\nu + \int_{4\pi} \kappa I_\nu d\Omega \right) d\nu, \quad (5.5)$$

with  $\nu$  the frequency. For the precise form of  $Q_{rad}$  for a DyI<sub>3</sub>-Hg mixture we refer to [35].

### Particle transport

Since we assume LTE, the particle densities may be described by the local temperature, pressure and elemental composition. Elemental pressure is defined as the pressure that contains all molecular, atomic and ionic contributions of a particular element. The elemental pressure  $p_\alpha$  for the element  $\alpha$  can be written as

$$p_\alpha = \sum_i R_{i\alpha} p_i, \quad (5.6)$$

with  $p_i$  the partial pressure of the species  $i$ , and  $R_{i\alpha}$  the stoichiometric coefficient [15]. We solve a conservation equation for the elemental pressure

$$\nabla \cdot \left( \frac{D_\alpha}{kT} \nabla p_\alpha + \frac{p_\alpha}{kT} \mathbf{c}_\alpha \right) = 0, \quad (5.7)$$

with an effective diffusion coefficient  $D_\alpha$  [15]

$$D_\alpha = p_\alpha^{-1} \sum_i R_{i\alpha} D_i p_i \quad (5.8)$$

and a pseudo convective velocity  $c_\alpha$  [15].

The diffusion coefficient  $D_i$  is calculated from the binary diffusion coefficients  $D_{ij}$  by

$$D_i = \left( \sum_{j \neq i} (p_j/p) / D_{ij} \right)^{-1}. \quad (5.9)$$

The binary diffusion coefficient for the diffusion of species  $i$  through species  $j$  is given by [36, page 486] and depends on the differential cross-section.

In-situ measurements of the elemental pressure at the walls under micro-gravity conditions are not possible, therefore we assume a Dy elemental pressure at the wall of 517 Pa and an I elemental pressure of 4268 Pa. These vapour pressures were determined with x-ray induced fluorescence measurements at 1g [10]. These are assumed to give a good estimation of the vapour pressure at the walls and used to fix the boundary conditions.

### Ohmic heating

The power to the plasma is supplied by ohmic heating. We solve the Poisson equation in the form:

$$\nabla \cdot (\sigma_{el} \nabla \Phi) = 0, \quad (5.10)$$

with  $\Phi$  the potential. From the potential  $\Phi$  we can derive the electric field  $\mathbf{E} = -\nabla\Phi$  and the current density  $\mathbf{J} = \sigma_{el}\mathbf{E} = -\sigma_{el}\nabla\Phi$ . The following boundary conditions are imposed:

1. There is no current through the walls, resulting in a homogeneous Neumann boundary condition ( $\frac{\partial\Phi}{\partial n} = 0$ ).
2. One electrode is kept at zero potential, which leads to a Dirichlet condition  $\Phi = 0$  at that electrode.
3. The potential of the other electrode is initially put at 100 V. This value is adjusted during the iteration process and determined by the fact that the power dissipated in the discharge equals 110 W. This is equivalent to the actual lamp power of 130 W of which 20 W is consumed by electrode losses and 110 W by ohmic dissipation of the discharge.

### The selection of cross-sections

In the basic equations, summarized in the previous section, important roles are played by various transport coefficients, such as the diffusion coefficients  $D_i$ , the thermal conductivity  $\lambda_c$  and the electrical conductivity  $\sigma_{el}$ . These transport properties are calculated from collision integrals that are based on differential cross sections [27].

Ideally, one would like differential cross-sections for every possible collision between particles in the plasma. In practice such data is difficult to gather or calculate since for only a few interactions energy-dependent integral cross-sections  $\sigma_{ij}$  are available. When available these are used in the model. For collisions for which such data cannot be found approximations have to be used. The collisions can be classified along the following categories:

1. Charged - charged collisions; in this case the shielded Coulomb cross-sections is a good and generally applicable approach [19, page 55],
2. Neutral - neutral collisions; there where dedicated cross-section values are not available these interactions are described as hard sphere collisions,
3. Charged - neutral collisions; this category is the most complicated since, in principle, a full quantum mechanical (QM) treatment is needed in which, for instance, the effect of the Ramsauer minimum has to be taken into account. For each pair of interacting particles the QM aspects are different. If results of experiments or QM calculation

are not available the use of the Langevin cross-section is the only option. The formula for the Langevin cross-section reads [17]

$$\sigma_{ij} = \sqrt{\frac{\pi\alpha_p q^2}{\mu_{ij}\epsilon_0 (|\mathbf{v}_i - \mathbf{v}_j|)}}, \quad (5.11)$$

with  $\alpha_p$  the dipole polarizability of the neutral species,  $q$  the charge of the charged species,  $\epsilon_0$  the permittivity of free space and  $\mu_{ij}$  the reduced mass  $\mu_{ij} = m_i m_j / (m_i + m_j)$  of the system of colliding particles.

When considering the influence of the cross-section on the values of the transport coefficients  $D_i$ ,  $\lambda_c$  and  $\sigma_{el}$  it is important to note that Hg atoms form the most dominant species in the discharge; all other species are present in small concentrations.

We begin with the electrical conductivity  $\sigma_{el}$  that is mainly determined by the elastic interactions between electrons with Hg atoms. This electron-Hg interaction is of the third category but fortunately the corresponding cross-section is well known and it is generally expected that the values from Rockwood [38] are correct within a few percent. We studied whether this is indeed the case by comparing the results using Rockwood values and Langevin cross-sections. As the value of this cross-section determines the lamp resistance and the ohmic dissipation we calculated the voltage drop over the lamp when the ohmic dissipation equals 110 W. This was done for two cases, one based on the Rockwood values and the other on the Langevin cross-section. Using the Rockwood values the model predicts a voltage drop of 99 V, which is consistent with the measured value. The calculations done with the Langevin cross-section, however, produces a voltage drop of 71 V, which is much too low. We may therefore conclude that the model gives a good description of the potential distribution over the lamp and the corresponding ohmic heating by using the Rockwood values.

Next we study the choice of cross-section for the thermal heat conductivity  $\lambda_c$ . Due to the low elemental concentration of Dy and I we can neglect the heat generation that is liberated in the formation of DyI<sub>x</sub> molecules. The reactive part of heat conductivity can therefore be neglected and only the frozen part remains (see [27]) which is determined by the collisions of Hg atoms mutually. These Hg-Hg collisions are of the second category and experimental results given in [36] confirm that the hard sphere approach is valid here.

Finally, we look at the diffusion of Dy. The diffusion of Dy containing species is determined by the collisions with Hg atoms. In case of the neutral species we deal with the second category for which the hard sphere approach can be used. Much less clear are the collisions between Hg atoms and Dy ions. These are of the third category and since there are no QM or experimental results available we have to use the expression of the Langevin cross-section. However, it is known from literature that this is not always a good approximation and errors in the order of 30% or more [39] are frequently reported. To study the impact of the  $\sigma(Hg, Dy^+)$ -value on the model results we performed two sets of calculations, one with the Langevin cross-section  $\sigma_{LV}$  and one with a value that is 20% larger, i.e.  $1.2 * \sigma_{LV}$ . In this way we can determine the importance of this Hg-Dy<sup>+</sup> cross-section and test the possible errors introduced by the approximation.

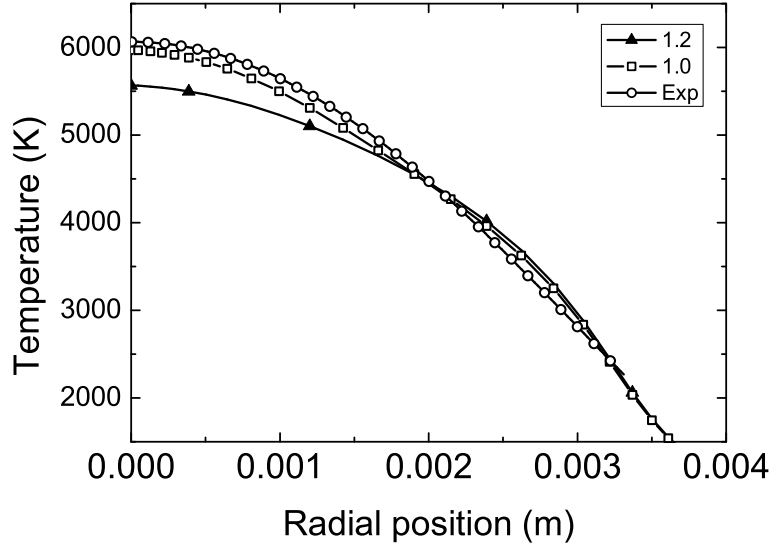


**Figure 5.5:** Radial temperature profile for a lamp containing 10 mg Hg and 4 mg DyI<sub>3</sub> at the midplane of the lamp. The numbers 1.0 and 1.2 refer to the two Langevin cross-sections that were used, the normal Langevin cross-section  $\sigma_{LV}$  and  $1.2 \cdot \sigma_{LV}$ . Exp denotes the experimental results.

## 5.5 Results and discussion

The experiment and model results are compared in this section. Both model and experiments were done for a lamp in micro-gravity, so without convection, operating at 130 W (of which 110 W dissipated in the discharge and 20 W spend on electrode losses) and containing 10 mg Hg and 4 mg DyI<sub>3</sub>. The sensitivity of the model results for the choice of  $\sigma(Hg, Dy^+)$  is examined. To that end two different cross-sections were used for the model, namely the Langevin cross-section  $\sigma_{LV}$  and  $1.2 \cdot \sigma_{LV}$ . This discussion will follow the line of the theory presented in section 5.3 where the three atomic systems were introduced, namely the Hg atom, the Dy ion and Dy atom. The Hg-system is used for the determination of the temperature, and the atomic and ionic Dy system for the spatial distribution of Dy atoms and ions and the radial Dy segregation.

### The temperature profile

The temperature profile as deduced from the Hg line is given in figure 5.5 and shows that the model based on the Langevin cross-section is in good agreement with the experiment. Both profiles have an axis temperature of 6000 K and nearly the same shape. If we take  $\sigma(Hg, Dy^+) = 1.2 \cdot \sigma_{LV}$  this results in a broader temperature profile with a lower axis

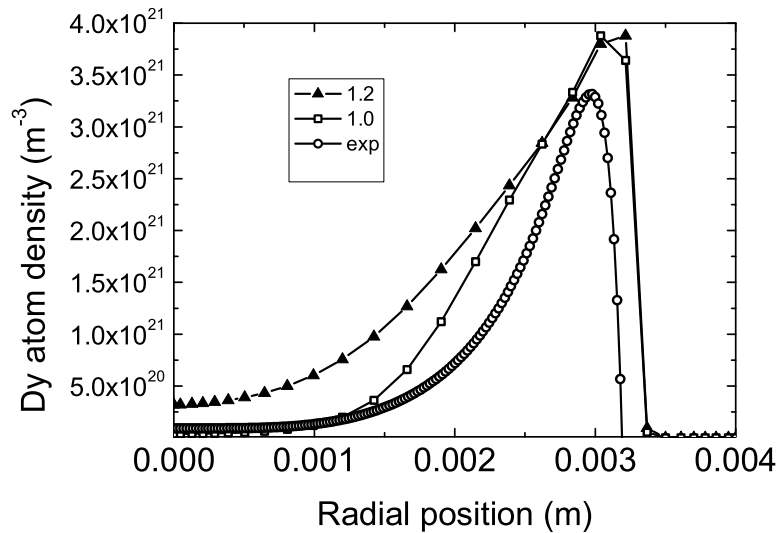


**Figure 5.6:** Radial Dy atom system density profile for a lamp containing 10 mg Hg and 4 mg DyI<sub>3</sub> at the midplane of the lamp. The numbers 1.0 and 1.2 refer to the two Langevin cross-sections that were used, the normal Langevin cross-section  $\sigma_{LV}$  and a value that is 20% larger:  $1.2 \cdot \sigma_{LV}$ . Exp refers the experimental results.

temperature. The reason why the higher  $\sigma(Hg, Dy^+)$  value influences the temperature profile is the following. By increasing  $\sigma(Hg, Dy^+)$  the ambipolar diffusion in the central region is being hampered which causes the Dy particles to be accumulated in the centre. The temperature then decreases slightly as Dy has a lower ionisation potential than Hg (5.93 eV versus 10.43 eV). However, the change in the temperature distribution remains in the error margin of 10% [9] so that no conclusions can be drawn about the optimum value for  $\sigma(Hg, Dy^+)$  from the temperature value.

## The Dy atom

Figure 5.6 shows the absolute system density of atomic Dy for both the experiment and two model results for  $\sigma(Hg, Dy^+) = \sigma_{LV}$  and  $\sigma(Hg, Dy^+) = 1.2 \cdot \sigma_{LV}$ . Both numerical and experimental curves have a steep slope at nearly the same radial position (about 3.3 mm) where the Dy atom associates into the DyI<sub>3</sub> molecule, see figure 5.2. The experimental curve has a steep slope partially because, in order for the Abel fit to yield physical results, the fit was forced to zero near the edges of the lateral profile [9]. It shows that the experimental and theoretical values of the maximum of the atomic Dy system agree with each other within 20%. This is in fairly good agreement in view of the fact that the uncertainty of the transition probability from which the density is determined is in the order 20%. Also important is the uncertainty related to the cold spot temperature. A small change in this

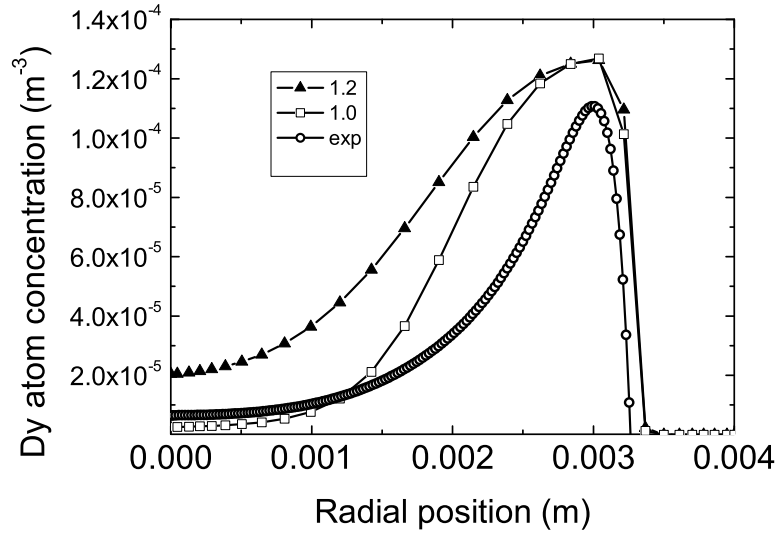


**Figure 5.7:** The atomic Dy concentration obtained by dividing the Dy atom density by the Hg density. The lamp contains 10 mg Hg and 4 mg DyI<sub>3</sub> at the midplane of the lamp. The numbers 1.0 and 1.2 refer to the two Langevin cross-sections that were used, the normal Langevin cross-section  $\sigma_{LV}$  and  $1.2 \cdot \sigma_{LV}$ . Exp denotes the experimental results.

temperature will lead to a significant variation of the elemental Dy density.

By dividing the Dy atom density by the Hg atom density distribution (which is the bulk species) the atomic Dy concentration is found, see figure 5.7. The atom concentration gives an indication of the radial segregation. The concentration profile clearly shows radial segregation for both experiment and model. Compared to the experiment, the model predicts more profound radial segregation. However, by increasing the cross-section from  $\sigma_{LV}$  to  $1.2 \sigma_{LV}$  we see that the theoretical central Dy concentration increases drastically; with more than a factor of 8. This implies that the amount of radial segregation is diminished and becomes much smaller than what is found experimentally. By increasing the cross-section, the diffusion is reduced, resulting in a decreased radial segregation.

The above clearly shows that the atom concentration at the centre is very sensitive to the choice of the cross-section; an increase of the cross-section by 20% leads to an increase of the central atomic density of a factor of 8.2 and the figure suggests that  $\sigma(Hg, Dy^+)$  will have a value somewhat larger than  $\sigma_{LV}$  but smaller than  $1.2 \cdot \sigma_{LV}$ . However, care should be taken with this theory-experiment comparison since the experimental values result from an Abel inversion which is quite sensitive for errors at the centre of a hollow profile.

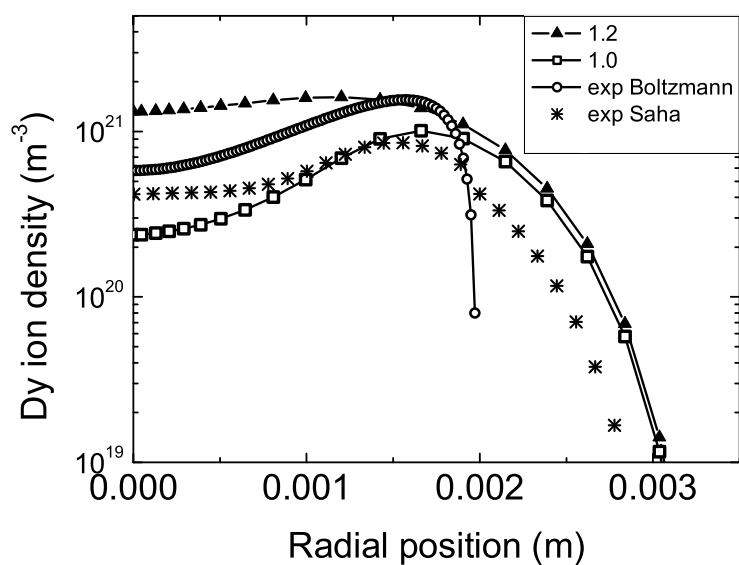


**Figure 5.8:** Radial Dy ion system density profile for a lamp containing 10 mg Hg and 4 mg  $\text{DyI}_3$  at the midplane of the lamp. The numbers 1.0 and 1.2 refer to the two Langevin cross-sections that were used, the normal Langevin cross-section  $\sigma_{LV}$  and  $1.2 \cdot \sigma_{LV}$ . Exp denotes the experimental results. The experimental value for the Dy ion density was determined by either Boltzmann, denoted as exp Boltzmann; or by Saha, then denoted by exp Saha.

## The Dy ion

The comparison of the model and experiment with respect to the Dy ion density is given in figure 5.8. We first focus on the central region where we find that, just as the Dy atom density, the theoretical value of central ion density is very sensitive to the value of  $\sigma(Hg, Dy^+)$ . The change from  $\sigma_{LV}$  to  $1.2 \cdot \sigma_{LV}$  leads to an increase of the central density with a factor 5.4. This is smaller than in the atomic case where a ratio of 8.2 is found.

The reason that both the Dy atom and ion density increase is that, as a consequence of the decrease in the ambipolar diffusion coefficient, the amount of Dy is more easily 'trapped' in the centre. This causes the temperature in the centre of the discharge to become lowered (as shown in figure 5.5) which as a result will cause the Saha balance between the atomic and ionic system to shift with respect to the atomic system. This is why the atomic Dy increases more strongly than the Dy ion as  $\sigma(Hg, Dy^+)$  is being increased.

Leaving the central region and moving outwards we see that the experimental Dy ion density in figure 5.8 has a much steeper slope than what the model predicts. In part this is caused by the Abel fitting as mentioned before. However, a more important aspect is the validity of LTE away from the centre. The experimental Dy ion density as shown in figure 5.8, denoted by "exp Boltzmann", is based on the application of the Boltzmann balance (equation 5.2) in the ionic system; this gives the Dy ion system density using the emission of a Dy ion line.

However, since the charge of the core of the ion system ( $Z = 2$ ) is twice as large as that of the atom system ( $Z=1$ ), we can expect that the transition frequency induced by electron collisions will be smaller (this scales as  $Z^{-2}$ ) [18] whereas the radiative decay transition (scaling as  $Z^4$ ) [18] will be higher than in a comparable atomic system. This means that as  $n_e$  decreases (in the direction toward the wall) the electron-ruled Boltzmann balance of excitation and de-excitation will no longer be in equilibrium. The spontaneous emission will then become the most dominant de-population process and the level is in the so-called Corona balance [18]. This causes the density of radiating states to decline. This implies that the ionic system density as deduced from these levels will decline as well.

We first investigate a possible departure from equilibrium by calculating the ion density using the Saha relation between the atomic and ionic system. This density is in fact based on the atomic radiation and thus the atomic system. For this system we can expect that, due to the lower  $Z$  value ( $Z=1$ ), it will not easily be effected by a drop in  $n_e$ . The Saha relation between  $n_i$ , the system density ion stage, and  $n_s$ , the system density of Dy atoms, reads

$$\frac{n_e n_i}{n_s} = 2 \frac{Q_i}{Q} \left( \frac{2\pi m_e k T}{h^2} \right)^{3/2} e^{-I_p/kT} \quad (5.12)$$

where  $Q$  is the partition function for the neutral species and  $Q_i$  the partition function for the ion,  $m_e$  the electron mass,  $T$  the temperature,  $I_p$  the ionisation potential of the atomic ground state,  $k$  the Boltzmann and  $h$  the Planck constant. The density of the Dy ion system can be found by inserting in this equation for  $n_e$  the sum of the Hg ion and the Dy ion density and for the atom density  $n$  the measured Dy atoms as shown in figure 5.6.

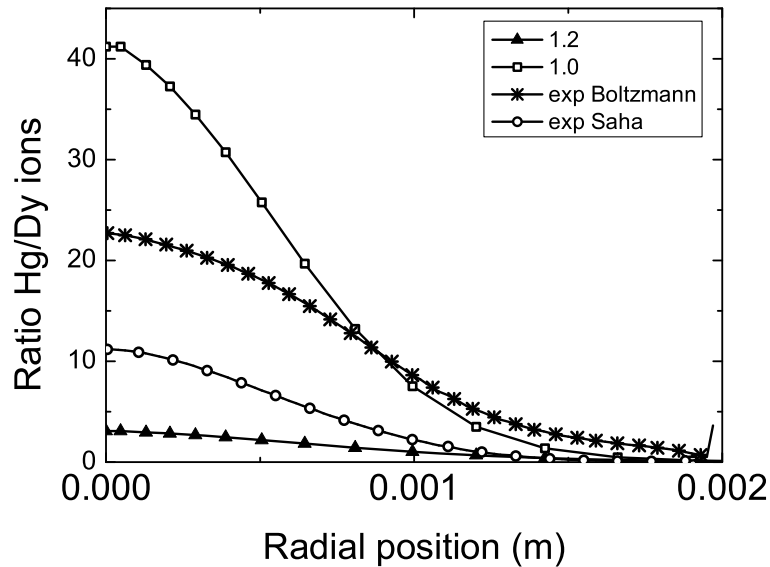


**Figure 5.9:** The Hg ion and Dy ion ratio for a lamp containing 10 mg Hg and 4 mg DyI<sub>3</sub> at the midplane of the lamp. The numbers 1.0 and 1.2 refer to the two Langevin cross-sections that were used, the normal Langevin cross-section  $\sigma_{LV}$  and  $1.2 \cdot \sigma_{LV}$ . Exp denotes the experimental results. The ratio is calculated from either the measured Dy ion density (calculated from Boltzmann) or from the measured Dy atom density (calculated from Saha).

The results of this equation given in figure 5.8, denoted with "exp Saha" show a much better agreement between the calculated ion density using Saha's equation and the model results in the outer region. In contrast to the curve found by employing the Boltzmann relation (equation 5.2), the Saha value of the ion system density declines more gradually in the outer region. There is a factor of 2 difference between the Saha calculation and the model results. This may be caused by a number of factors. First, there is more atomic Dy in the model than in the real lamp as was shown in figure 5.6. Second, there may be an error in the transition probability, leading to an error in the atom density calculated with equation 5.2. Finally, an error may be introduced by the Abel inversion.

### The Hg/Dy ratio

As stated above in dealing with the Saha equation, we have to take  $n_e$  equal to the sum of the Hg ion and the Dy ion density<sup>1</sup>. In contrast to commercial lamps with PCA tubes for which the Dy vapour pressure is higher than in our model lamp used in the experiments we can not neglect the contribution of the Hg ions. In fact it was found experimentally from

<sup>1</sup>this was not the case in [8] and [9], where  $n_e = n_{Hg+}$

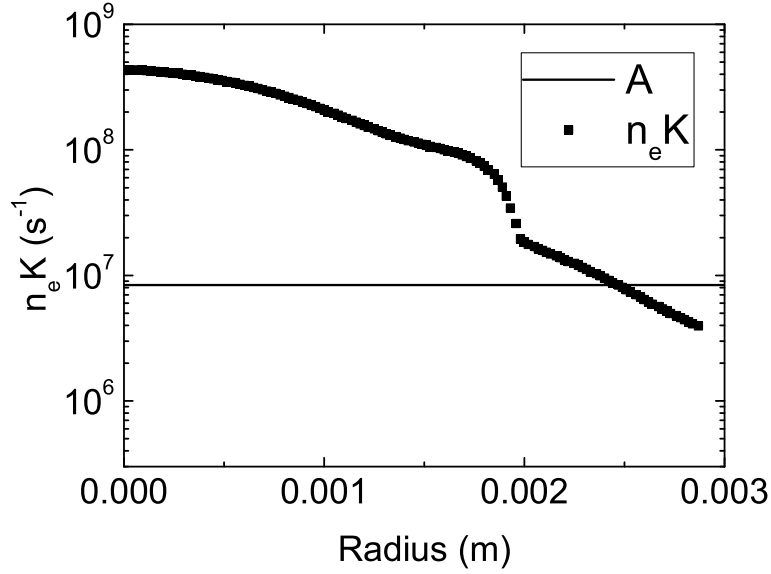


**Figure 5.10:** The collision frequency  $n_e K$  compared to the radiative frequency which is represented by the transition probability  $A$ .

the  $\text{Hg}^+/\text{Dy}^+$  ion ratio [9] that the Hg ions dominate in the centre, see figure 5.9 where the experimental values of the  $\text{Hg}^+/\text{Dy}^+$  ratio are given. Two ratio's are shown, one of which the Dy ion calculation is based on Boltzmann (cf. equation 5.2) the other of which the calculation is based on Saha (cf. equation 5.12). These are compared to two model results based on  $\sigma(\text{Hg}, \text{Dy}^+) = \sigma_{LV}$  and  $\sigma(\text{Hg}, \text{Dy}^+) = 1.2 \cdot \sigma_{LV}$ .

It is clear the model predicts the ratio  $\text{Hg}^+/\text{Dy}^+$  to be high for a normal Langevin cross-section. At higher cross-section ( $1.2 \cdot \sigma_{LV}$ ) this ratio is much lower, as there are more Dy ions in the centre (cf. figure 5.8). A higher cross-section causes Dy ions to be accumulated in the centre so that the central temperature will decrease. This will radically reduce the number of Hg ions, as they have a much higher ionisation potential.

It can be concluded from the above that the  $\text{Hg}^+/\text{Dy}^+$  ion ratio is the most effective parameter for finding the optimum value of  $\sigma(\text{Hg}, \text{Dy}^+)$  when comparing the results of the model with that of the experiment. An advantage of using the ion ratio is that the Abel inversion is more reliable for the Dy ion than for the atom as the latter contains a hollow structure. Figure 5.9 suggests that the best value of the  $\sigma(\text{Hg}, \text{Dy}^+)$  will in the order of  $1.1 \cdot \sigma_{LV}$ .

## Departure from LTE

We now return to the topic of the rapid decay in the  $\text{Dy}^+$  density at  $r=0.002$  m as shown in figure 5.8, which was found using Boltzmann's law. The Dy ion system density is

determined by that of an excited Dy ion state which decreases rapidly due to the sudden decrease of the electron density. This under-population of the excited Dy ions has been previously reported [8] and is, as mentioned before, expected near the wall where the number of electrons is dramatically reduced. This causes the Boltzmann balance to shift to a Corona balance and this leads to a departure in LTE. A deviation from LTE in the outer region of the discharge has already been observed for the high pressure sodium lamp [40].

The transition from the Boltzmann-Saha balance to the Corona balance, happens when the collision frequency  $n_e K_p$  is about equal to the radiative frequency (i.e. transition probability)  $A_p$ .

$$n_e K_p \simeq A_p \quad (5.13)$$

where  $A_p$  and  $n_e K_p$  are the rates for total radiative and collisional destruction. We estimate the collision frequency by treating the Dy ion as hydrogen-like. The collision rate can then be written as [18]

$$K_p = 4\pi a_0^2 (p/Z)^4 \left( \frac{3kT}{m_e} \right)^{1/2} \quad (5.14)$$

where  $a_0$  is the Bohr radius,  $Z$  the charge number of the core (which is 2 for the ion) and  $m_e$  the electron mass. The effective principal quantum number  $p$  of the level in question is calculated from  $Z\sqrt{Ry/E_p}$  with  $Ry$  the Rydberg energy and  $E_p$  the ionisation potential of the level in question (thus in this case the energy needed for Dy<sup>2+</sup> formation) [18]. For  $A_p$  we use the radiative transition probability of  $A_p = 8.4 \cdot 10^6 \text{ s}^{-1}$  as used in the experiment.

The results are depicted in figure 5.10. It shows that the assumption of LTE is no longer valid after  $r/R > 50\%$ . This results in the excited Dy ions to be underpopulated. An under-population of the excited states with respect to Boltzmann means that equation 5.2 will underestimate the density of the ions. Thus we have found deviations from LTE. However, this departure of LTE only has a limited effect on the main plasma parameters such as the temperature and the electron density. It will also not change the spectrum emitted by the plasma substantially. This means that using an LTE model is justified to describe the phenomena in this type of lamp. When we calculate the threshold in equation 5.13 for the Dy atom we find that the Boltzmann balance still holds.

It should be realized that in the way we employ equation 5.13 a hydrogen-like system is assumed and we thus ignore the fact that the Dy ion has much more lower lying levels that will facilitate step-wise excitation instead of direct excitation from the ground level. For a proper description of the experimental results a full collisional radiative model would be needed which is beyond the scope of this study.

## 5.6 Conclusions

There is a reasonable agreement between model and experiment. The model is based on the following elementary parameters, the electrical conductivity is based on the electron-Hg cross-section from Rockwood, the thermal conductivity is determined from hard-sphere

collisions and the Hg-Dy<sup>+</sup> collisions are determined from the Langevin cross-sections. The temperature profiles are in good agreement and are not very sensitive to the Langevin cross-section. Dy atom profiles show an abrupt transition between atom and molecule for both model and experiment. The comparison between the experiment and model results for the Dy atom concentration shows that the model predicts more radial segregation.

The ratio  $Hg^+/Dy^+$  was found to be extremely sensitive for the cross-section of the elastic interaction  $\sigma(Hg, Dy^+)$  between  $Dy^+$  and Hg atom. The sensitivity analysis reveals that equating  $\sigma(Hg, Dy^+)$  to a value that is 10% higher than the Langevin cross-section is the best choice. There is a clear discrepancy between experiment and the LTE-based model for the Dy ion density profiles. The experiment shows the Dy ion density to decrease much more rapidly. Further analysis showed deviations from LTE in the outer regions of the plasmas for relative radial positions of  $r/R > 50\%$ . These deviations are manifest in the excited part of the  $Dy^+$  system that for relatively low  $n_e$  is ruled by the Corona rather than by the Boltzmann balance. However, this departure of LTE only has a limited effect on the main plasma parameters which means that using an LTE model is justified.

In order to also study the effect of convection, experiments have also been done at hyper-gravity [11] and normal gravity [10], the future plan is to compare numerical results of the model to these experiments.



---

## Bibliography

---

- [1] Waymouth J, Electric discharge lamps, MIT press, Cambridge, 1971
- [2] Coaton J R, Marsden A M, Lamps and Lighting, Arnold, London, 4th edition, 1997
- [3] Lister G G, Lawler J E, Lapatovich W P and Godyak V A 2004 Rev. Mod. Phys. **76**, 541
- [4] Fischer E 1976 J. Appl. Phys. **47**, 2954
- [5] Zhu X 2005 Ph.D. thesis, Eindhoven University of Technology
- [6] Flikweert A J, Van Kemenade M, Nimalasuriya T, Haverlag M, Kroesen G M W and Stoffels W W 2006 J.Phys.D **39**, 1599
- [7] Flikweert A J, Nimalasuriya T, Groothuis C H J M, Kroesen G M W and Stoffels W W 2005, J. Appl. Phys. **98** 073301
- [8] Nimalasuriya T, Pupat N B M, Flikweert A J, Stoffels W W, Haverlag M and Van der Mullen J J A M 2006 J. Appl. Phys. **99** 053302, **see chapter 2**
- [9] Nimalasuriya T, Flikweert A J, Haverlag M, Kemps P C M, Kroesen G M W, Stoffels W W, Van der Mullen J J A M 2006 *J. Phys D: Appl Phys* **39** 2993, **see chapter 3**
- [10] Nimalasuriya T, Curry J J, Sansonetti C J, Ridderhof E J, Shastri S D, Flikweert A J, Stoffels W W, Haverlag M, Van der Mullen, J J A M 2007 J.Phys.D **40**, 2831, **see chapter 6**
- [11] Nimalasuriya T, Thubé G M, Flikweert A J, Haverlag M, Kroesen G M W, Stoffels W W, Van der Mullen 2007, J.Phys.D 2007 **40** 2839, **see chapter 4**
- [12] Stoffels W W, Baede A H F M, Van der Mullen J J A M, Haverlag M and Zissis G 2006 Meas. Sci. Technol. **17** N67
- [13] Benoy D A, 1993 *Modelling of Thermal Argon Plasmas* PhD Thesis Eindhoven University of Technology, the Netherlands
- [14] Van Dijk J 2001 *Modelling of plasma light sources* PhD Thesis Eindhoven University of Technology, the Netherlands
- [15] Beks M L, Hartgers A, Van der Mullen J J A M 2006 J.Phys.D **39**, 4407
- [16] Beks M L, Van Dijk J, Hartgers A, Van der Mullen J J A M accepted for publication
- [17] Lieberman M A, Lichtenberg A J 1994, *Principles of Plasma Discharges and Materials Processing*, Wiley & Sons, New York
- [18] Van der Mullen J J A M 1990 Phys. Rep. **191** 109

- [19] Mitchner M and Kruger Jr C H 1973 *Partially ionized gases*, 1st ed., (John Wiley and Sons).
- [20] Kemps P C M, 2004 An experimental study of the radial additive density and plasma temperature profiles, and the effect of this on the integral light output of metal-halide lamps as a function of gravity *Master's thesis* Eindhoven University of Technology
- [21] Kroesen G M W, Haverlag M, Dekkers E, Moerel J, de Kluijver R, Brinkgreve P, Groothuis C H J M, Van der Mullen J J A M, Stoffels W W, Keijser R, Bax M, Van den Akker D, Schiffeleers G, Kemps P C M, Van den Hout F H J, Kuipers A 2005 *Microgravity sci. technol.* XVI-1
- [22] Stoffels W W, Haverlag M, Kemps P C M, Beckers J and Kroesen G M W 2005 *Appl. Phys. Lett.* **87** 1
- [23] Atomic Line Data (Kurucz R L and Bell B) Kurucz 1993 CD-ROM No. 23. Cambridge, Mass.: Smithsonian Astrophysical Observatory
- [24] Wickliffe M W and Lawler J E 2000 *J. Quant. Spectrosc. Radiat. Transfer* **66**, 363
- [25] [http://www.thespectroscopynet.com/Theory/Partition\\_Functions.asp](http://www.thespectroscopynet.com/Theory/Partition_Functions.asp)
- [26] Van der Heijden H W P, Van der Mullen J J A M 2002 *J. Phys. D* **35**, 2112
- [27] Johnston C W, Van der Heijden H W P, Van der Mullen J J A M 2002 *J. Phys. D* **35**, 342
- [28] Bellows A H, Feuersanger A E, Rogoff G L, and Rothwell H L, 'HID convection studies: a space shuttle experiment,' 1984 Illuminating Engineering Soc. Meeting
- [29] Bellows A H, Feuersanger A E, Rogoff G L, and Rothwell H L, 'Convection and Additive segregation in High pressure lamp arcs: Early results from a space shuttle experiment,' 1984 Gaseous electronics Conf., 1985 *Bull. Amer. Phys. Soc.* Vol **30**, p 141
- [30] Elenbaas W 1951 *The high pressure mercury vapour discharge*, 1st ed., (North-Holland publishing company)
- [31] Fischer E 1978 *Influences of External and Self-Magnetic Fields on the behaviour of discharge lamps*, Philips GmbH Forschungslaboratorium Aachen Lobornotiz nr 13/78.
- [32] Curry J J, Sakai M and Lawler J E 1998 *J. Appl. Phys.* **84**, 3066
- [33] Benck E C, Lawler J E and Dakin J T 1989 *J. Opt. Soc. Am. B* **6**, 11
- [34] Stoffels W W, Kroesen G M W, Groothuis C H J Mv, Flikweert A J, Nimalasuriya T, Van Kemenade M, Kemps P C M, Bax M, Van den Hout F H J, Van den Akker D, Schiffelers G, Beckers J, Dekkers E, Moerel J, Brinkgreve P, Haverlag M, Keijser R and Kuipers A 2005 *Proceedings of the XXVIIth International Conference on Phenomena in Ionised Gases Eindhoven (16-342)*, july 17-22, 2005, E.M. Van Veldhuizen, Eindhoven University of Technology.
- [35] Beks M L, Van der Mullen J J A M, to be submitted
- [36] Hirschfelder J O, Curtiss C F and Bird R B 1966, *Molecular Theory of Gases and Liquids*, 3rd edition, (John Wiley and Sons Inc.)
- [37] Chapman S and Cowling T G 1970 *The Mathematical Theory of Non-uniform Gases*, Cambridge University press third edition
- [38] Rockwood S D 1973, *Phys. Rev. A.*, **8** 2348
- [39] Chen C L Raether M 1962 *Phys. Rev.* **128** 2679

- [40] de Groot J, Van Vliet J 1986, *the high pressure sodium lamp*, Philips technical library, kluwer technische boeken, Deventer, Antwerpen